Geochemistry Geophysics Geosystems G3

Article
Volume 14, Number 7
30 July 2013
doi: 10.1002/ggge.20170
ISSN: 1525-2027

Published by AGU and the Geochemical Society

Variability of internal frontal bore breaking above Opouawe Bank methane seep area (New Zealand)

Hans van Haren
Royal Netherlands Institute for Sea Research (NIOZ), AB Den Burg, Netherlands Royal Netherlands Institute for Sea Research (NIOZ), PO Box 59, NL-1790 AB Den Burg, Netherlands (hans.van.haren@nioz.nl)

Jens Greinert
Royal Netherlands Institute for Sea Research (NIOZ), AB Den Burg, Netherlands

GEOMAR Helmholtz Centre for Ocean Research Kiel Wischhofstrasse, Kiel, Germany

[1] Large internal wave breaking is observed exceeding a vertical array of 61 high-resolution temperature sensors at 1 m intervals between 7 and 67 m above the bottom. The array was moored for 5 days at 969 m of Opouawe Bank, New Zealand, a known methane seep area. As breaking internal waves dominate sediment resuspension above sloping topography in other ocean areas, they are expected to also influence methane transport. Despite being visible in single beam echosounder data, indications for turbulence due to rising gas bubbles are not found in the present 1 Hz sampled temperature records. Likely, the mooring was too far away from the very localized bubble release spot. Instead, the temperature sensors show detailed internal wave-turbulence transitions. Every tidal cycle, a solibore (a frontal turbulent bore with a train of trailing solitary waves) changes shape and intensity. These solibores are highly turbulent and they restratify the bottom boundary layer, thereby maintaining efficient mixing. Details of different turbulent bore developments are discussed. Averaged over a few tidal cycles and over the sensors range, mean vertical eddy diffusivity amounts to $3 \pm 1 \times 10^{-3}$ m^2 s^{-1} and mean turbulent kinetic energy dissipation to $1.6 \pm 0.7 \times 10^{-7}$ W kg^{-1}, with variations over 4 orders of magnitude. Such turbulence will affect the distribution of dissolved methane and other geochemical species in the lower 100–150 m above the bottom and their release from the bottom. The above mean values are remarkably similar to those found at various other sites in the NE Atlantic Ocean.

Components: 6,829 words, 9 figures.

Keywords: large internal wave breaking; methane seep area; high-resolution temperature observations; different solibore developments; Opouawe Bank New Zealand.

Index Terms: 4211 Oceanography: General: Benthic boundary layers; 4544 Oceanography: Physical: Internal and inertial waves; 3004 Marine Geology and Geophysics: Gas and hydrate systems.

Received 12 October 2012; **Revised** 2 May 2013; **Accepted** 5 May 2013; **Published** 30 July 2013.

van Haren, H., and J. Greinert (2013), Variability of internal frontal bore breaking above Opouawe Bank methane seep area (New Zealand), *Geochem. Geophys. Geosyst.*, *14*, 2460–2473, doi:10.1002/ggge.20170.

1. Introduction

[2] Understanding the different transport mechanisms of methane released from the sea floor into the ocean is vital to accurately judge if and under which conditions natural oceanic methane sources from natural hydrocarbon seepage, decomposing gas hydrate, as well as leaking gas wells and pipelines will have an increasing effect on atmospheric methane concentrations. Convectively rising bubbles locally create turbulence in the water column thereby disturbing its temperature structure [*McGinnis et al*., 2004]. Depending on the strength of the bubble release, such turbulence varies accordingly and these variations can be used to trace the active periods of the bubble induced upwelling of methane-rich water [*Leifer et al*., 2006]. On the other hand, "internal waves," which are supported by the vertical density stratification, and turbulence generated by their breaking at sloping topography over likely much larger scales than those of bubble plumes have never been investigated as potentially important mechanism and might have to receive the same scientific attention for gas transport as bubble release [*Leifer et al*., 2006; *Rehder et al*., 2009; *Greinert et al*., 2010].

[3] Methane seepage has been described from quite a few continental margin settings around the world since the early 1980s. Active seepage is commonly identified offshore Svalbard as "flares" in acoustic echograms [e.g., *Westbrook et al*., 2009]. Video observations have proved that these flares are indeed created by bubbles [*Fisher et al*., 2011]. However, quantitative measurements on the amounts of turbulence generated have not been made so far. Recent studies using bottom landers and a 24 h conductivity-temperature-depth (CTD) yoyo station showed that methane release and its distribution is strongly dependent on currents, tides, and internal waves (Greinert, unpublished data).

[4] At the Hikurangi Margin offshore New Zealand as in many other seep areas around the world, elevated methane concentrations can be observed across the entire water column through convection. However, highest concentrations are often limited up to 200 m above the bottom [*Heeschen et al*., 2005; *Sauter et al*., 2006; *Westbrook et al*., 2009; *Faure et al*., 2010]. At some seep sites off New Zealand, strong acoustic backscattering was found in acoustic Doppler current profiler data (ADCP) to vary more or less with tidal periodicity and rising typically 50–60 m above the bottom [*Linke et al*., 2010]. This strong backscattering was interpreted to be caused by episodically released bubbles. Such episodic bubble release has been visually observed during remotely operated vehicle dives at several seep sites of the Hikurangi Margin [*Naudts et al*., 2010] and elsewhere [e.g., *Schneider et al*., 2010, 2011].

[5] However, in the deep sea, strong acoustic backscatter is also typical for internal wave breaking above sloping topography in the form of "solibores" consisting of a frontal turbulent internal bore and a train of nonlinear internal solitary waves of elevation. This is because solibores generate large sediment resuspension [*Klymak and Moum*, 2003; *Hosegood et al*., 2004; *Bonnin et al*., 2006]. They reach up to 50 m from the bottom, thereby creating a large turbulence scale in the stratified water, with their associated vertical currents having amplitudes O (0.1 m s^{-1}) observed at least twice as high. The leading edge of the solibores passes a fixed observer's position within minutes while their trailing waves generate decaying turbulence up to several hours after their passage [*Klymak et al*., 2008]. In most tidally dominated areas above sloping topography, their time of passage varies by about 10% of the time of a tidal period [*van Haren*, 2006]. They are sometimes followed by a second, weaker, and less turbulent solibore [*van Haren and Gostiaux*, 2012]. Because of their capability of creating large turbulent overturns and their ubiquity in the world's oceans, it may thus well be that internal waves also dominate dissolved gas transport in particular if gas release sites are located on sloping seabed. Sloping bottoms are also the primary location of internal wave generation and breaking.

[6] The mixed fluids generated by breaking internal waves at sloping topography spread along isopycnals, thereby affecting the overall stratification in the ocean interior, e.g. [*Armi*, 1978]. This is because the ocean, despite being stably stratified in density from surface to bottom mainly by near-surface solar radiation, also requires substantial turbulent mechanical mixing to maintain deep stratification [*Munk and Wunsch*, 1998]. This mixing is thought to be predominantly induced by internal wave breaking [*Thorpe*, 1987a; *Gregg*, 1989], a partial sink for tidal energy. Internal tides are generated via the interaction of horizontal motions with sloping underwater topography, in a model ocean with continuous (constant) stratification most efficiently where the bottom slope "critically" matches the wave slope. Thus, it is conjectured that most mixing through internal wave breaking also occurs above (critical) topography, because of the focusing of wave energy, rather than above flat bottoms or in

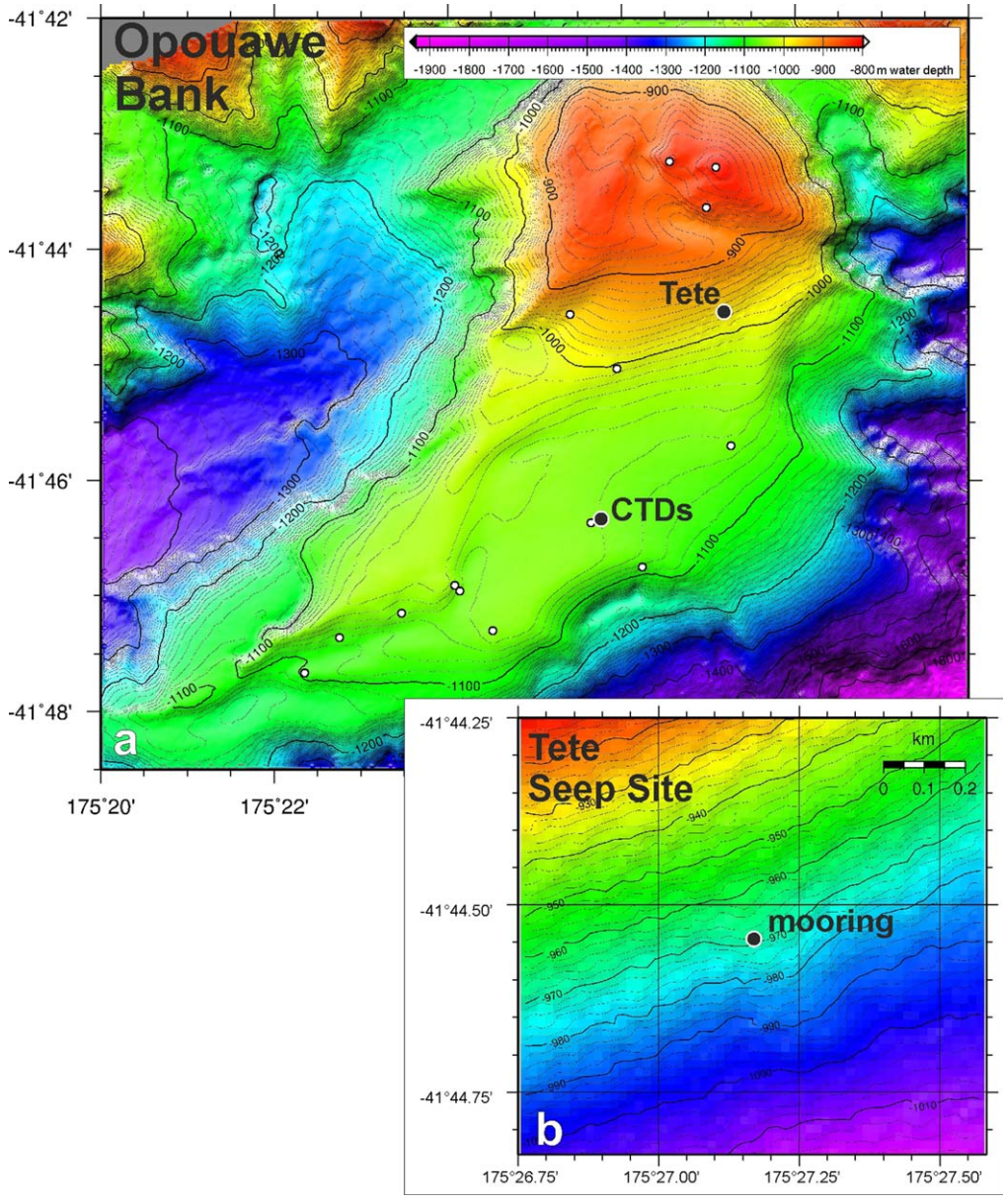

Figure 1. (a) Opouawe Bank mooring area to the southeast of New Zealand, northern island. This relatively deep bank is an area with many known methane gas seeps (open circles), of which (b) mooring area Tete is at about 970 m water depth on a southward dipping slope. Note the color levels are different from those in Figure 1a. Water depth is indicated by the contour lines.

the interior of the water column [*Munk*, 1966; *Armi*, 1978; *Thorpe*, 1987b; *Garrett*, 1990, 1991]. Numerical modeling suggests internal wave induced mixing above all slopes including dub- and supercritical ones [*Legg and Adcroft*, 2003]. If such internal wave induced mixing above sloping topography is efficient enough, it may suffice to represent the basinwide vertical turbulent diffusivity (K_z), presently rated at $K_z = 10^{-4}$ m^2 s^{-1}, needed to maintain the vertical density stratification [*Munk and Wunsch*, 1998].

[7] Here we present detailed observations using vertically densely spaced, high sampling rate and high-precision temperature sensors in a mooring above a known methane seep site off Cape Palliser at the southern tip of New Zealand's North Island (Figure 1). The advantage of using these sensors above acoustics is that they can be used to quantitatively estimate turbulence parameters [*van Haren and Gostiaux*, 2012]. Comparison of data from colocated acoustic instrumentation (ADCP) and data from such temperature sensors has shown

that both are adequate to detail internal wave frontal bores [*van Haren*, 2009]. The objectives of this paper are to investigate the possibility of using high sampling rate thermistors to quantify turbulence induced by processes like rising bubbles and internal wave breaking and their effects on methane redistribution in the water column next to seep sites. In addition, the observations are used in the larger ocean-scale study on the effects of mixing above sloping boundaries for the maintenance of the overall vertical density stratification in the ocean interior.

2. Materials, Background Conditions, and Methods

[8] A total of 61 "NIOZ4" self-contained temperature (T) sensors were used sampling at 1 Hz, with precision better than 0.001°C and a noise level of about 6×10^{-5}°C. All sensors worked as anticipated for the 5 days of mooring. NIOZ4 is an upgrade of NIOZ3 [*van Haren et al.*, 2009], with similar characteristics, except for its reduced size (2/3 smaller) and reduced power consumption (with the capacity of sampling at a rate of 2 Hz for the duration of 1 year). Sensors were taped at 1.0 m vertical intervals to a nylon-coated steel cable, with the lowest sensor 7 m above the bottom and the upper about 2.5 m below a single elliptic floatation providing 2000 N of net buoyancy. The sensors were synchronized via induction every 6 h. Thus, timing mismatch was less than 0.04 s. This taut-wire mooring was deployed from 10 to 15 April 2011 at the Tete seep site of Opouawe Bank, Hikurangi Margin, New Zealand (Figure 1) [*Greinert et al.*, 2010]. Its position was 41°44.544′S, 175° 27.177′E, $H = 969$ m water depth, and very near a gas flare according to ship's echosounder (Figure 2). The high (fisheries) risk of the area did not allow for a longer mooring duration, with the research vessel out of the area.

[9] The electromagnetic 120 12 kHz multibeam bathymetry (Figure 1b) based local bottom slope was $\gamma = 0.094$ (5.4°), see also the map of slopes in Figure 3a. Using local CTD observations (Figure 4) to determine a "mean" large-scale buoyancy frequency $N = 3 \pm 1 \times 10^{-3}$ s^{-1} (computed using 10 profiles obtained at different times in the area and using a vertical scale of 100 m directly above the bottom), we compare this slope with that of potential internal wave ray slopes $\beta = \sin^{-1}((\sigma^2 - f^2)^{1/2}/(N^2 - f^2)^{1/2})$, for internal wave ($\sigma$) and inertial ($f$) frequencies, in an environment of constant N. The 100 m vertical averaging scale of this mean buoyancy is adequate to resolve the height (twice the amplitude) of the largest internal waves. It is thus equivalent to averaging over other large internal wave scales: 1–10 km in the horizontal and 1 day in time. It is noted that the above uncertainty in N is mainly due to natural variations in the density field, partially caused by internal waves passing with their straining giving rise to smaller-scale stratification and interfacial internal waves, and only marginally attributable to instrumental errors. Over a scale of 100 m, N can be measured down to an instrumental error of 7×10^{-5} s^{-1} in near-homogeneous waters, as has been verified experimentally by *van Haren and Millot* [2006]. Freely propagating internal waves are in the range $f \sim< \sigma \sim< N$. For the dominant semidiurnal lunar tidal frequency M_2 we find mean $\beta = 0.034 \pm 0.011$ (1.9 ± 0.6°). The local bottom slope is thus found $\gamma > \beta$, or supercritical for internal tides, significant to within 95% uncertainty. Critical slopes are found about a kilometer or one internal tidal wavelength both to the north and, especially, to the south of the mooring (Figure 3b). Known seep sites mostly are found at all bottom slopes, super, sub, and critical. The main CTD station is in the center of a large subcritical slope area, and it is noted that N is valid for the 10×10 km range of Figure 3.

[10] Hydrographically, the CTD data from a single station to the southwest of the mooring (41° 46.14′S, 175° 25.74′E) on day 104.6 (15 April around 16 UTC) show that temperature dominates density variations over most of the lower half of the local water column (Figures 4a–4c). The weaker salinity contributions are generally negative, in terms of static stability, except deeper than 900 m (in this profile) when it contributes positively. The aforementioned large-scale buoyancy frequency supports shortest period (highest frequency) internal waves having periods down to $T_N = 1500$ s. In detail, small-scale layering down to $\Delta z = 1$ m gives a maximum $N_{1,\max} = 10^{-1.7}$ s^{-1} computed over $\Delta z = 1$ m or a minimum small-scale internal wave period down to $(T_{N1})_{\min} = 300$ s.

[11] Temperature sensor data are first transferred to conservative temperature (Θ) values [*McDougall et al.*, 2009; *TEOS*, 2010], before they are used as an estimate for (variations in) potential density anomaly referenced to a level of 1000 dBar (σ_{1000}) following a reasonably tight, constant

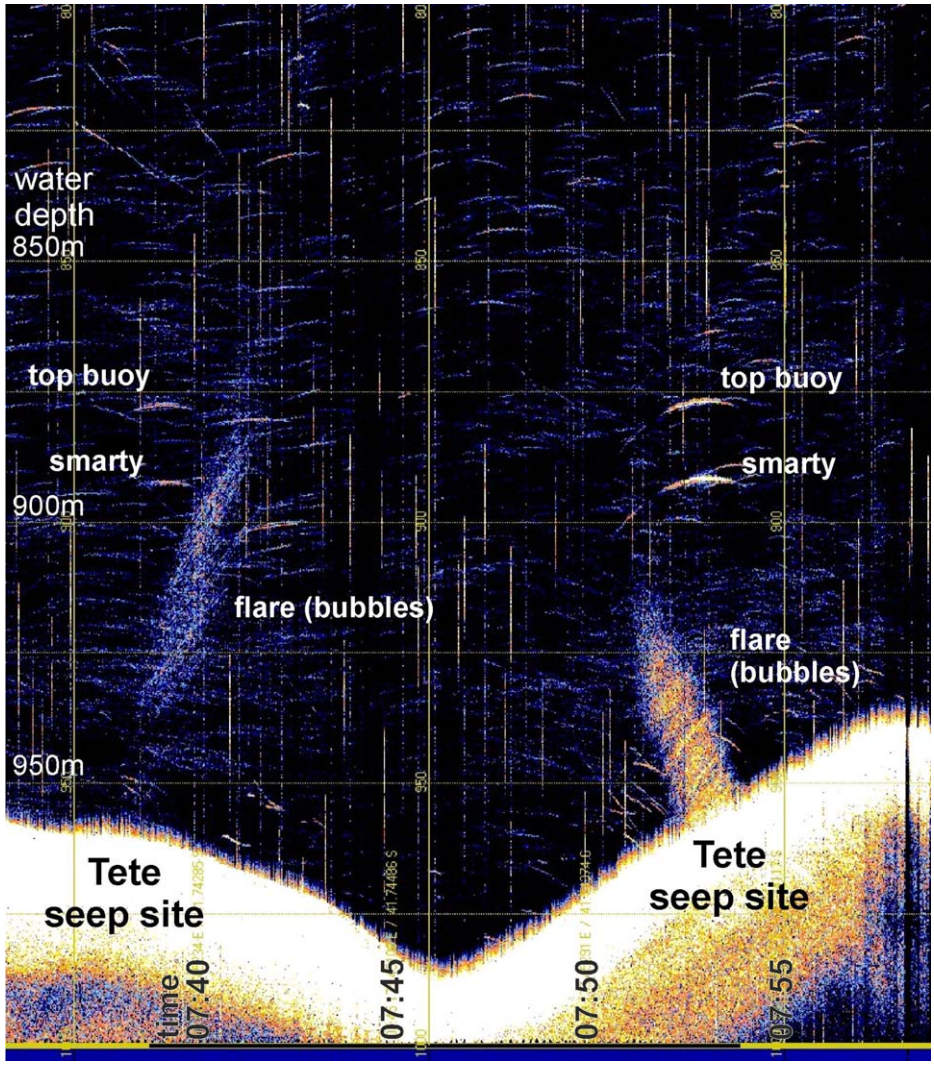

Figure 2. Echogram (18 kHz, Parasound primary frequency) sailed twice, with a turning in the middle, showing the top (pickup line) buoy and the main floatation ("smarty") as reflections in the water column. The mooring was positioned very close to the Tete flare.

linear relationship obtained from CTD (Figure 4e), $\delta\sigma_{1000} = \alpha\delta\Theta$, $\alpha = -0.15 \pm 0.01$ kg m^{-3}°C^{-1} denoting the thermal expansion coefficient under local conditions. This relationship is the mean for the lower 100 m above the bottom from five CTD-profiles around the main site (Figure 1a). During periods of weaker turbulence $\alpha = -0.14$, while during stronger near-bottom turbulence $\alpha = -0.16$ (cf., Figure 4e). Henceforth, we will use the above "tight" mean relationship to estimate turbulence parameters using the moored temperature sensor data. Care will be taken to recognize layers of density compensated temperature inversions. These layers are relatively easily detectable in detailed turbulence parameter images and are excluded from the turbulence estimates (see below).

[12] The Θ data are used to estimate vertical turbulent eddy diffusivity K_z and turbulent kinetic energy dissipation rate ε by calculating "overturning" scales. These scales are obtained after reordering (sorting) every 0.5 s the 60 m high potential density (conservative temperature) profile, which may contain inversions, into a stable monotonic profile without inversions [*Thorpe*, 1977, 1987a]. As *Thorpe* [1987b] mentioned, the recognizing of overturns is more precise in temperature than in combined temperature-salinity (i.e., density anomaly) data, because of the increased noise levels when using two sensors instead of one and because of the problem of sensor mismatch, although the latter is much improved in SeaBird's pumped SBE911 CTD sensors. As done by *Klymak et al.*

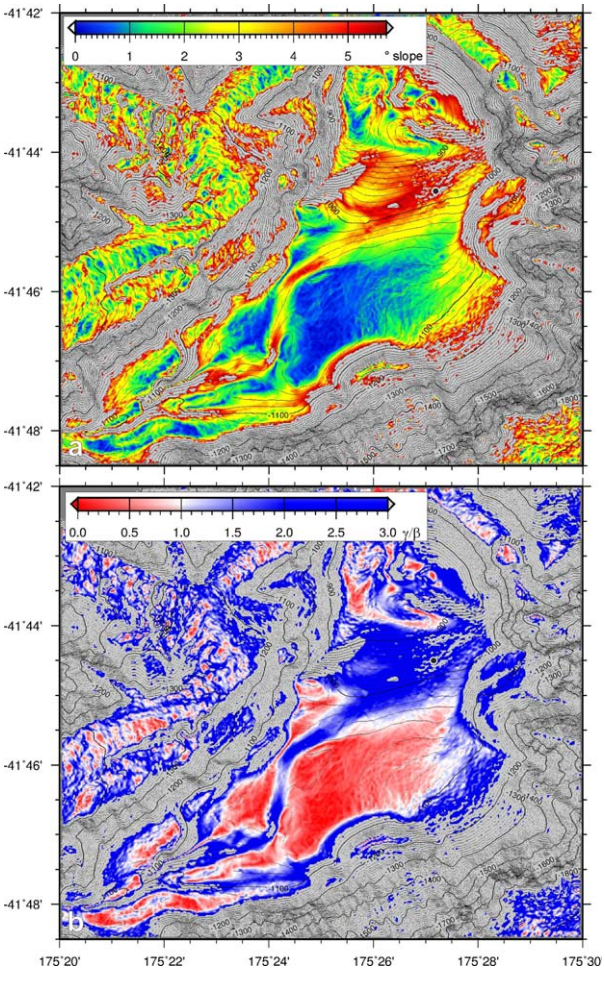

Figure 3. Multibeam data from map in Figure 1a to calculate bottom slopes on a 50 m grid using GMT. (a) Bottom slopes in degrees. Gray when the slope exceeds 6°. (b) Ratio of angles of bottom slope over internal tidal wave slope using a mean large-scale N, determined from the lower 100 m above the bottom from five CTD-profiles around 1060 m water depth (Figure 1a) and approximately valid for the 10 × 10 km area of the figure. White indicates critical slopes, blue supercritical slopes, and red subcritical slopes.

[2008], we verified this using our SBE911 CTD data. Turbulence parameter estimates from CTD-temperature-only and from CTD-density anomaly data were found equivalent to within 20%. This corresponds in general with the findings by *Klymak et al*. [2008]. We are thus confident to use the moored temperature sensor data to estimate turbulence parameter given the above density-temperature relationship. The moored sensors have an advantage over CTD and microstructure profilers: profilers need 1–2 min to descend (obliquely) through a 60 m range instead of sampling overturns instantaneously (to within 0.04 s). After comparing observed and reordered profiles, displacements (d) are calculated necessary for generating the reordered stable profile. A certain threshold applies to disregard apparent displacements associated with instrumental noise and post-calibration errors. This threshold is very low for NIOZ-temperature sensor data, $<5 \times 10^{-4}$°C [*van Haren et al*., 2009]. Then,

$$\varepsilon = 0.64 d^2 N^3, \quad (1)$$

where N denotes the buoyancy frequency computed from each of the reordered, essentially statically stable, vertical density profiles. The numerical constant follows from empirically relating the overturning scale with the Ozmidov scale $L_O = 0.8d$ [*Dillon*, 1982]. Using $K_z = \Gamma \varepsilon N^{-2}$ and a constant mixing efficiency of $\Gamma = 0.2$ [*Osborn*, 1980; *Klymak et al*., 2008] for conversion of kinetic into potential energy, we find

$$K_z = 0.128 d^2 N. \quad (2)$$

[13] In (1) and (2), we use individual d to replace overturning scales, rather than taking their RMS value across a single overturn as originally proposed by *Thorpe* [1977]. The reason is that we cannot easily distinguish individual overturns, first, because overturns are found at various scales with small ones overprinting larger overturns, precisely as one expects from turbulence, and, second, because some exceed the range of temperature sensors. Instead, we first calculate nonaveraged d in (1) and (2) for high-resolution images of $K_z(z, t)$ and $\varepsilon(z, t)$. Subsequently, we calculate "mean" turbulence parameter values by averaging the parameters in the vertical [] or in time <>, or both. The errors in the mean turbulence parameter estimates thus obtained depend on the error in N, the error in the temperature-density relationship while the instrumental noise error of the thermistors is negligible (see above). Given the above errors, the estimated uncertainty in time-depth mean estimates of (1) and (2) amount about a factor of 2. Using similar temperature sensor data from Great Meteor Seamount, *van Haren and Gostiaux* [2012] found turbulence parameter estimate values to within a factor of 2 similar to those inferred from ship-borne CTD/LADCP profiler data near the bottom. They also performed several tests using different averaging of turbulence parameters. It was found that simple averaging of K_z yielded no significantly different results from the averaging of vertical density (heat) fluxes $-K_z \rho / g N^2$ ($K_z \mathrm{d}\Theta/\mathrm{d}z$) and N first, before arriving at average K_z.

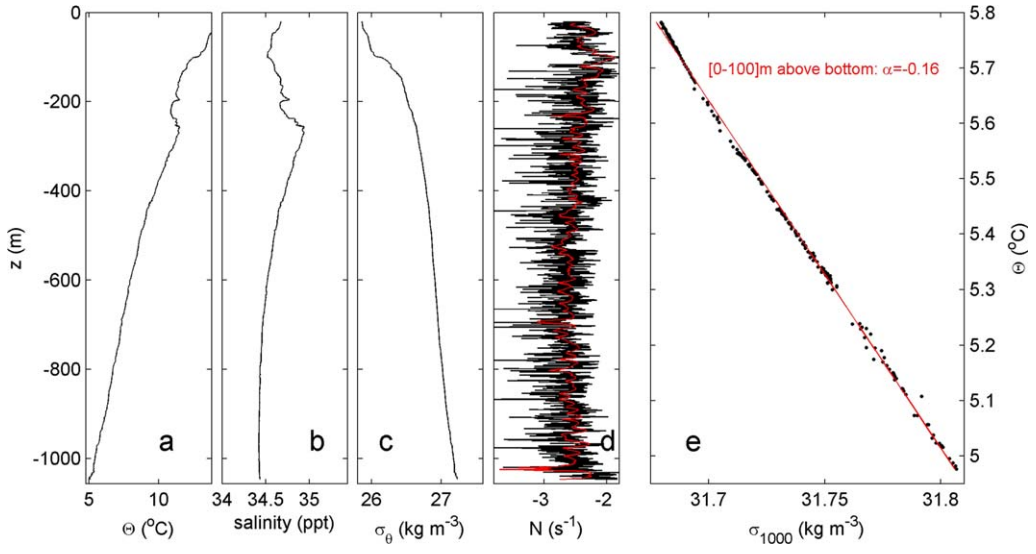

Figure 4. Overview of hydrographic data obtained 3 km southwest of the mooring site (Figure 1a). CTD profile obtained on day 114.6, immediately after recovery of the mooring. (a) Conservative temperature. (b) Absolute salinity. (c) Potential density anomaly ($\sigma_\theta = \rho - 1000$, ρ density) referenced to the surface. (d) Buoyancy frequency, computed over 1 m (black) and 10 m (red) vertical scales. (e) Potential density anomaly referenced to 1000 dBar–conservative temperature relationship. The straight line is for $\delta\sigma_{1000} = -0.160 \pm 0.001\delta\Theta$ kg m^{-3}.

3. Observations

[14] Careful inspection of the full depth-time record shows no signs of bubble-induced turbulence in the entire 5 day record of temperature sensor data. This is of course not visible in the overview of Figure 5, but it is also not visible in the much more detailed plots that will be presented below.

[15] Although no indications of bubbles or their induced turbulence have been observed in the temperature sensor data, some vigorous internal wave breaking has been seen. Solibores occur once or twice in a tidal period and more or less at tidal periodicity, despite the noncriticality of the bottom slope for internal tides. After calibration and drift correction (typically 0.001°C/week), the data show a dominant tidal periodicity (Figure 5a).

[16] The first half of the record (up to day 101.4) shows regularly large temperature instabilities (when denser cold water is above warm water) with a duration significantly longer than the buoyancy period (Figure 5d). These apparent instabilities are not mainly caused by turbulence but due to salinity compensated inversions. This is also visible in the unusually high "background" turbulence parameter values (Figures 5e and 5f), and thus their smaller range of variations over 2 instead of 4 orders of magnitude for vertical averages monitored over a tidal period (Figure 5e). This observation leads to the hypothesis of a sharp distinction between internal waves and turbulence. Motions having periods larger than the local buoyancy period $(T_{NI})_{\min}$ are dominated by statically stable waves, whereas motions having periods shorter than $(T_{NI})_{\min}$ are mainly turbulent in character.

[17] The distinction between the two periods before and after day 101.4 probably has to do with a change in currents advecting different water masses, as evidenced from the substantially cooler waters moving in (Figure 4a), over the 60 m vertical range of temperature observations. It is not surprising that over such a small vertical range the T-S relationship remains very tight with a few days in time, as in Figure 4e. Such T-S persistence is typical for both temperature dominated water masses that are typical for the majority of ocean waters [*Stommel*, 1993; *Schmitt*, 1999] as well as for heterogeneous ocean conditions across multiple fronts of small- and mesoscale eddies in strongly convective areas were salinity-compensated conditions prevail [*Rudnick and Ferrari*, 1999; *van Haren and Millot*, 2009].

[18] The remainder of the present record is little affected by salinity-compensated temperature inversions, and overturns observed in temperature can be used as tracer for density overturns and thus for turbulence parameter estimates. This may

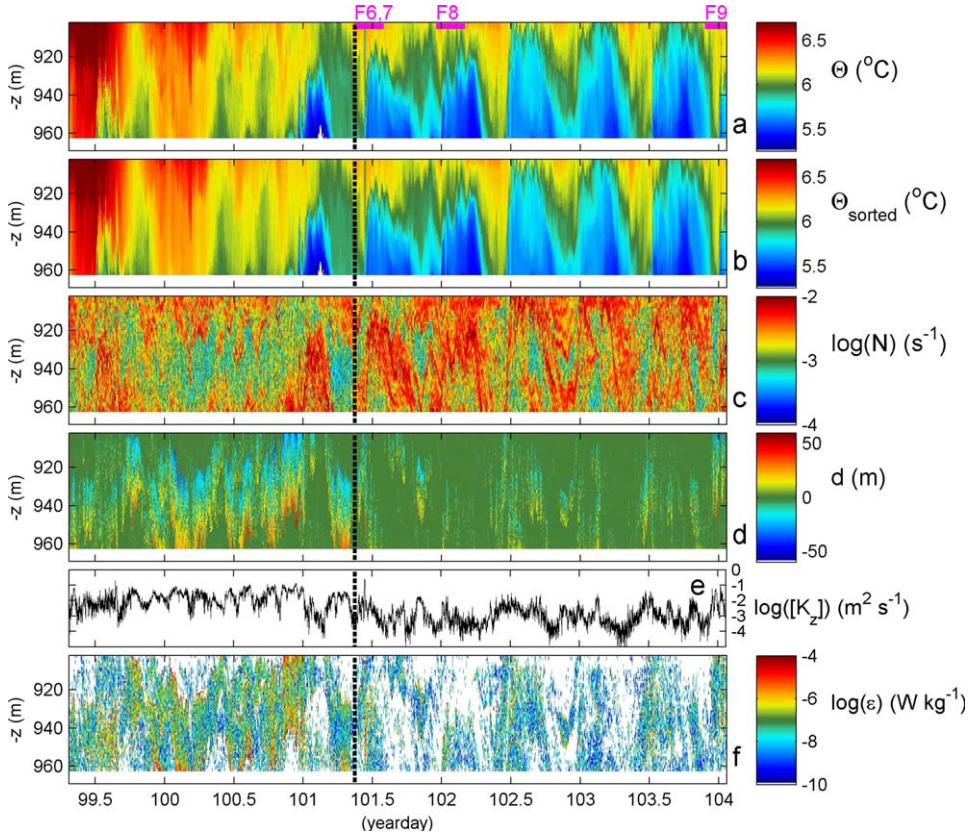

Figure 5. Overview of depth-time series of nearly 5 days in April 2010, using 61 NIOZ4 temperature sensors at 1 m intervals between 7 and 67 m above the bottom. Tidal variation is clearly visible, with amplitudes exceeding the vertical range of temperature sensors. In more detail, high-frequency internal waves and strongly nonlinear internal tidal waves are visible, of which details will be highlighted in subsequent figures of which the periods and numbers are indicated in purple. There is a change in water masses after day 101.4 (vertical dashed line), after substantially cooler waters move in, and intrusions (salinity inversions) are little important. (a) Observed data, transferred to conservative temperature [*TEOS*, 2010]. (b) Stable stratification after reordering Figure 5a to stable profiles every time step. (c) Stratification based on reordered data. (d) Overturning displacements following comparison of Figure 5a with its reordered data. (e) Time series of vertically averaged eddy diffusivity (logarithmic scale) using (2) and the relationship $\delta\sigma_{1000} = -0.15\delta\Theta$. (f) Turbulence dissipation rate, estimated using (1), logarithmic scale. White also indicates values below threshold.

already be inferred from the overall picture that shows some real spikes in turbulence parameter data, e.g., on day 101.45 (Figure 5).

[19] Zooming in (Figure 6) a large eddy diffusivity of $[K_z] = 1.5 \pm 1 \times 10^{-1}$ m^2 s^{-1} can be seen caused by a >65 m high nonlinear internal wave breaking. Its steep front passes nearly all the sensors within 3 min (see also Figure 7). Behind the large breaking wave trails, a set of 10–60 min lasting periodic internal waves (Figure 6). The frequency of these waves matches that for thin-layer stratification buoyancy frequency waves: $\sigma \sim N_{1,\max}$. This maximum internal wave frequency, or minimum period $(T_{N1})_{\min}$, de(in)creases with time commensurate the spreading of thin layers due to mixing. These waves border a core of highly turbulent motions included at the stratified edges. They last some 2 h after the big wave passed. The thin, strongly stratified edges above and below a turbulent core carry most of the vertical current shear [e.g., *van Haren*, 2007]. As the turbulent core, with typical $[K_z] = 10^{-3}$–10^{-2} m^2 s^{-1} is generally closer to the bottom than the prefront turbulence, the thin layer stratification is split with the lower edge within a few meters from the bottom (not very well visible in the present data).

[20] Such a vigorous event is not associated with gas bubble clouds being released, but typical for nonlinear (tidal) fronts breaking on deep-sea slopes [*Hosegood et al.*, 2004; *Klymak et al.*,

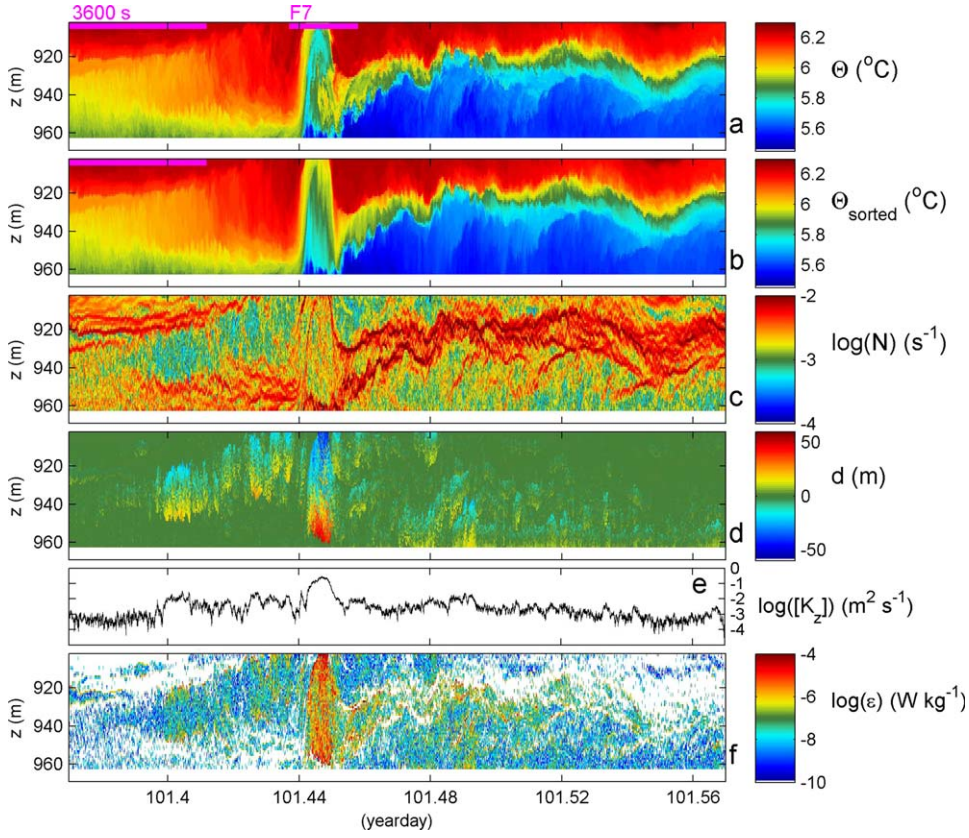

Figure 6. As Figure 5, but for 5 h detail around the transition from warming (downslope moving) to cooling (upslope moving) tidal phase, including a strong solibore: a frontal bore and train of trailing high-frequency internal waves. (a and b) Note the difference in scale compared with Figures 5a and 5b.

2008; *van Haren and Gostiaux*, 2012]. The short, but intense mixing events dominate sediment resuspension in this case, sweeping material at least 65 m upward in the water column. Given the typical extent of vertical currents, material might be "scooped up" more likely 100–150 m above

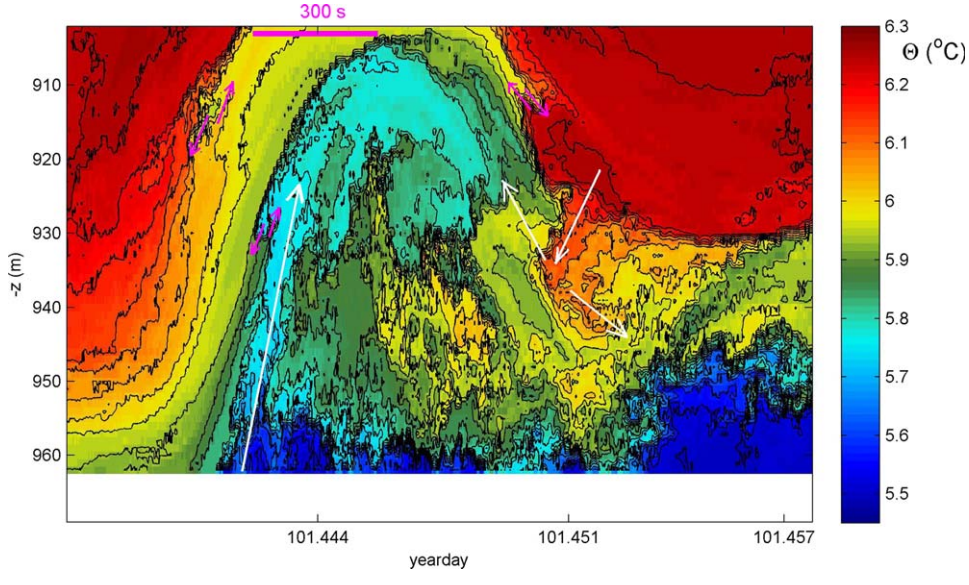

Figure 7. Half hour zoom of front in Figure 6, including temperature contours every 0.04°C.

the bottom which could not be monitored do to the length of the temperature array.

[21] The present frontal passage and trailing high-frequency internal waves follow more or less the common solibore-like passage of the upslope propagating phase of a tidal wave, as sketched in section 1. However, compared with NE Atlantic data the prefrontal stratification does not deepen as much here. The stratification stays about 10 m from the bottom (note the lowest sensor is at 7 m above the bottom), where <1 m has been observed previously [*van Haren and Gostiaux*, 2012]. Also, the turbulence away from the bottom is not very strong with values of $[K_z] = 10^{-3} - 10^{-2}$ m^2 s^{-1}and $[\varepsilon] = 10^{-8} - 10^{-7}$ W kg^{-1}. Previously, *van Haren and Gostiaux* [2012] suggested a correspondence between large prefrontal turbulence and frontal sharpness. Here, the front itself may still appear rather smooth and not very turbulent, but its height and interior core are vigorously turbulent despite the rather weak prefront turbulence (Figures 6e and 6f). The trailing split of stratification is not observed and the near-bottom enhanced stratification may be invisible in the nonsampled 7 m near the bottom.

[22] Zoomed in, some new features of internal wave breaking are shown in Figure 7. It is seen that the front is not smooth but shows indents of filaments of fluid passing each other. These indents are different from the little steps between days 101.442–101.444 and 910–930 m, separating 5.75 from 5.95°C waters. These steps are caused by the 1.0 m vertical separation between sensors and a very thin oblique front passing. The indents, e.g., around 914 m at days 101.441 and 101.449 (double purple arrows), are evidence of small-scale counter currents that oppose the main flow of the backward-breaking wave. Thus, these indents are caused by local shear, the start of small-scale overturns right at the largest stratification. This is observed all the way along the rim of the main wave, until behind the first breaker, where the main flow is split in two directions, forward and backward. Furthermore, shear indents and turbulent motions are found in the core at all scales down to the 1 m resolution.

[23] Not all fronts are like the one passing around day 101.44. The next tidal phase, around day 101.95, shows a very smooth wave passing (Figure 8). Apparently, this wave does not move strictly upslope but approaches more obliquely the sloping bottom as the front is not steeply developed. No interior prefrontal conditioning is observed. After the front passage, turbulence is generated, but the contrast with the previous front itself is substantial. Stratification initially remains more or less smoothly layered down to about 20–30 m from the bottom. Most intense turbulence occurs at the rim of stratification capping the large turbulent core. Here, small-scale overturns are visible in the temperature data. Such "rim turbulence" was also visible in Figure 6, behind the first big breaking wave.

[24] A few tidal periods later toward the end of the record, the front around day 104.005 shows another example of different solibore development passing the sensors (Figure 9). Its prefrontal development is typical because of the close bottom approximation of large stratification, which is pushed down by vigorous overturning away from the bottom. The overturns occur in two major groups, about half an hour apart for the duration of 1.2 h, and within these groups their intensity varies every 400–500 s. This periodicity of intensity variations is about a factor of 1.5 smaller than the smallest buoyancy frequency observed, under the assumption that the mean density-temperature relationship is valid. As noted above from CTD observations, salinity may contribute positively in thin layers, up to a 30% shorter period of freely propagating internal waves. Hence, temperature is here underestimating turbulence parameters. In spite of the rather strongly turbulent "preconditioning" of pushing the stratification close to the bottom, the initial front appearing about 15 min later is not well developed and reaches only about 30 m above the bottom. It does show a few small shear intrusions along its rim (e.g., Figure 9a, black arrow). However, as in Figure 8, after the first buoyancy period "wave" a further larger overturn reaches up to 50 above the bottom, followed by 300 s period overturns, commensurate the shortest thin-layer buoyancy period. Only after the passage of this "second front" higher up at which highest $\varepsilon = 10^{-4}$ W kg^{-1} is observed, the common split in two stratified layers is observed. This contrasts with Figures 6 and 8 in which this split was (marginally) seen after the first front.

[25] As for the intermittent occurrence of fronts, the large frontal bores appear with a periodicity of 0.5098 ± 0.033 days ($n = 6$) between days 101 and 104, when salinity did not hamper a tight density-temperature relationship. These values are halfway semidiurnal lunar (periodicity 0.517) and solar (0.5000) tidal periods. Their range of variation is about 1.5–2 times larger than found in previous strictly semidiurnal lunar mean data as in mainly upslope propagating fronts around 1500 m in the

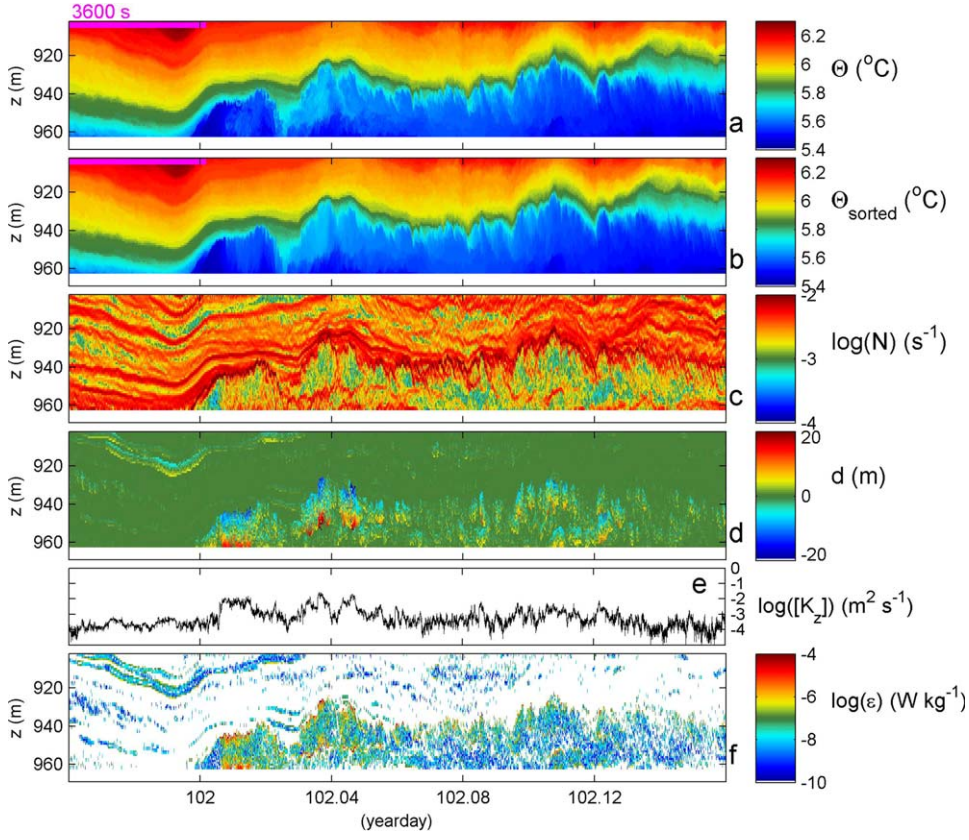

Figure 8. As Figure 6, but for next tidal "front" passage. (a,b, and d) Note the difference in scale compared with Figures 6a, 6b, and 6d.

Bay of Biscay, 0.515 ± 0.015 days ($n = 5$), or around 550 m water depth above Great Meteor Seamount NE Atlantic Ocean, 0.517 ± 0.020 days ($n = 11$) [*van Haren*, 2006]. This suggests that offshore New Zealand stratification varies over a wider range resulting in a slightly broader internal wave band. The wider range may also have to do with the relatively large number (three out of six) of obliquely propagating waves not fully developing a solibore, which makes the exact timing of the "frontal passage" difficult. Longer deployment times would be required to allow more precise conclusions. As was found at previous North Atlantic sites, strong vertical currents associated with the fronts having amplitudes of typically 0.1 m s^{-1} and having their vertical extent well exceeding the fronts may contribute significantly to the generation of (nonlinear) internal tides at the source.

4. Discussion

[26] The turbulence parameter values averaged over the period between days 101.4 and 104.06 and over the range of sensors between 7 and 67 m above the bottom, $<[K_z]> = 3 \pm 1 \times 10^{-3}$ m^2 s^{-1}, $<[\varepsilon]> = 1.6 \pm 0.7 \times 10^{-7}$ W kg^{-1}. Turbulence parameters are found to vary over 4 orders of magnitude in the original 0.5 s, 1 m time-depth resolution. Such a variation is typical for turbulence in natural waters [e.g., *Gregg*, 1989; *Lorke*, 2007; *van Haren and Gostiaux*, 2012]. These mean values are within 10% similar to data using similar sensors averaged over 18 days and between 0.5 and 50 m above the bottom (at 549 m) above Great Meteor Seamount, NE Atlantic Ocean [*van Haren and Gostiaux*, 2012]. They are also within a factor of 2 similar to estimates from a sloping boundary around 500 m water depth in the Faeroe-Shetland Channel [*Hosegood et al*., 2005] and around 1000 m above the Hawaiian Ridge [*Klymak et al*., 2008]. This may be a coincidence, noting that the large-scale stratification is approximately the same (to within 20%) at these sites, which are 200–300 m below the local morphological high. However, the correspondence suggests a universality of internal wave-induced turbulence generation above sloping topography, as the present site is not only

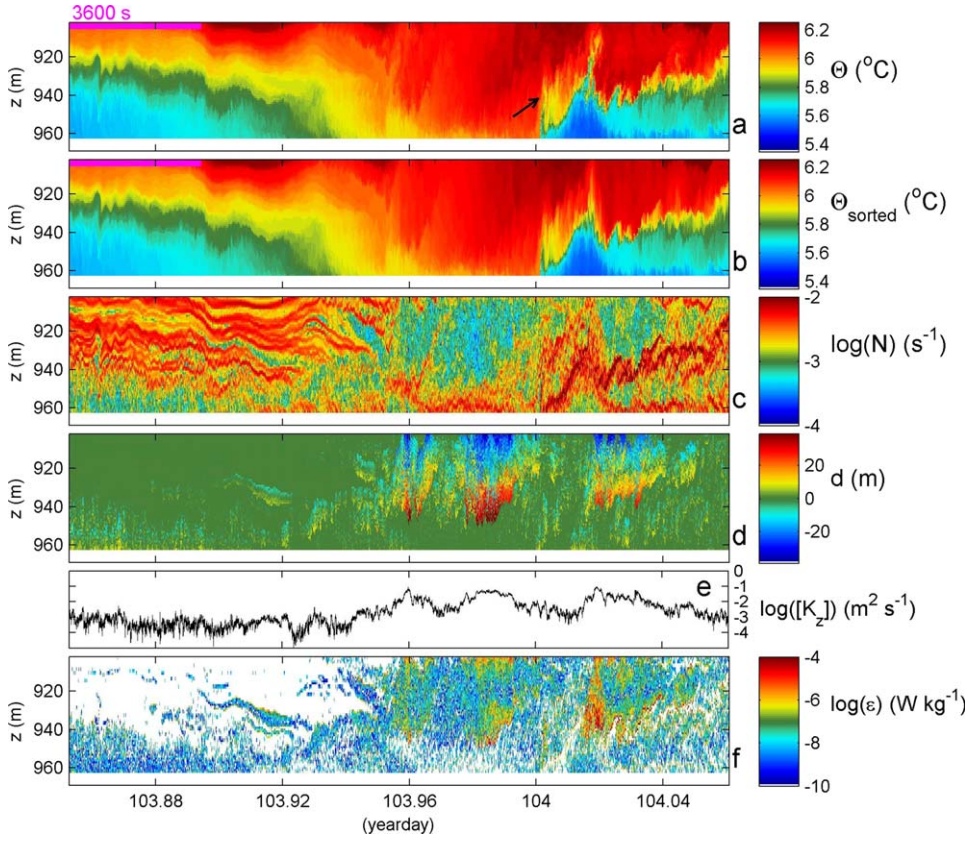

Figure 9. As Figure 6, but near the end of the record for a "double" front of which the first around day 104.00 (arrow) and a secondary jet higher up in the water column around day 104.02. (a, b, and d) Note the difference in scale compared with Figures 6a, 6b, and 6d.

twice as deep as the others, but its slope is also twice as steep, thereby significantly noncritical (supercritical) for internal tides. This appearance of different fronts, also at other sites between 100 and 3000 m deep [*Klymak and Moum*, 2003; *Hosegood et al*., 2004; *van Haren*, 2006; *Bonnin et al*., 2006; *Klymak et al*., 2008] further supports the importance of boundary mixing for global ocean vertical exchange, to maintain the overall density stratification as suggested by *Munk and Wunsch* [1998]. As internal waves continuously restratify the sloping boundary layer by their movements back and forth, rather than creating a large homogeneous layer as by steady alongslope flows, they maintain a high mixing efficiency. The above also suggests that breaking waves are less well described by a wave model of constant *N* focusing energy at a critical slope than by solibores propagating at interfaces and not affected by focusing.

[27] As conjectured by *van Haren and Gostiaux* [2012] and also visible in the present data, more than half of the mixing in a tidal period occurs within 30 min of the main solibore passage. Of this half, about a third occurs in the first 3 min of the actual largest front passage. This is, provided the front is well developed and propagating perpendicular to the slope. Such fronts and their intermittent appearance varying by 10% of the main [tidal] period may thus well have been observed by *Linke et al*. [2010] in their ADCP echo intensity data. It has been verified using acoustic and optical backscatter data and sediment trap data by *Hosegood et al*. [2004] and *Bonnin et al*. [2006] that these fronts dominate sediment resuspension. The question is, suppose they do so above Opouawe Bank, what would be the consequence for gas transport? Would it facilitate the methane transport from the bottom, explaining the more or less simultaneous increases of dissolved methane seen in geochemical data with increased acoustic backscatter found by *Linke et al*. [2010]? If so, it will certainly help to distribute methane much quicker and higher up in the water column by its turbulent mixing.

[28] Unfortunately, we found no direct evidence of free gas release (turbulence) in the present temperature sensor data. Perhaps bubble stream areas are too localized to be detected with such sensors, compared to internal wave breaking. More elaborate experiments with these sensors combined with acoustic devices, video footing and extensive gas analyses of water samples are foreseen for the near future.

Acknowledgments

[29] We thank captain and crew of R/V *Sonne* for their assistance during cruise SO214, 2nd leg. We greatly thank Martin Laan for design and construction of NIOZ temperature sensors and assistance in mooring preparation. NIOZ-MTM prepared the remainder of the mooring and took care of transportation. Bruce Sutherland revived the distinction between interfacial and continuous stratification internal waves.

References

Armi, L. (1978), Some evidence for boundary mixing in the deep ocean, *J. Geophys. Res.*, *83*, 1971–1979.

Bonnin, J., H.van Haren, P. Hosegood, and G.-J. A. Brummer (2006), Burst resuspension of seabed material at the foot of the continental slope in the Rockall Channel, *Mar. Geol.*, *226*, 167–184.

Dillon, T. M. (1982), Vertical overturns: A comparison of Thorpe and Ozmidov length scales, *J. Geophys. Res.*, *87*, 9601–9613.

Faure, K., J. Greinert, J. Schneider von Deimling, D. F. McGinnis, R. Kipfer, and P. Linke (2010), Methane seepage along the Hikurangi Margin of New Zealand: Geochemical and physical evidence from the water column, sea surface and atmosphere, *Mar. Geol.*, *272*, 170–188.

Fisher, R. E., et al. (2011), Arctic methane sources: Isotopic evidence for atmospheric inputs, *Geophys. Res. Lett.*, *38*, L21803, doi:10.1029/2011GL049319.

Garrett, C. (1990), The role of secondary circulation in boundary mixing, *J. Geophys. Res.*, *95*, 3181–3188.

Garrett, C. (1991), Marginal mixing theories, *Atmos. Oceans*, *29*, 313–339.

Gregg, M. C. (1989), Scaling turbulent dissipation in the thermocline, *J. Geophys. Res.*, *94*, 9686–9698.

Greinert, J., K. B. Lewis, J. Bialas, I. A. Pecher, A. Rowden, D. A. Bowden, M. De Baist, and P. Linke (2010), Methane seeps along the Hikurangi margin, New Zealand: Overview of studies in 2006 and 2007 and new evidence from visual, bathymetric and hydroacoustic investigations, *Mar. Geol.*, *272*, 6–25.

Heeschen K. U., R. W. Collier, M. A. de Angelis, E. Suess, G. Rehder, P. Linke, and G. P., Klinkhammer (2005), Methane sources, distributions, and fluxes from cold vent sites at Hydrate Ridge, Cascadia Margin, *Global Biogeochem. Cycles*, *19*, GB2016, doi:10.1029/2004GB002266.

Hosegood, P., J. Bonnin, and H. van Haren (2004), Solibore-induced sediment resuspension in the Faeroe-Shetland Channel, *Geophys. Res. Lett.*, *31*, L09301, doi:10.1029/2004GL019544.

Hosegood, P., H. van Haren, and C. Veth (2005), Mixing within the interior of the Faeroe-Shetland Channel, *J. Mar. Res.*, *63*, 529–561.

Klymak, J. M., and J. N. Moum (2003), Internal solitary waves of elevation advancing on a shoaling shelf, *Geophys. Res. Lett.*, *30*(20), 2045, doi:10.1029/2003GL017706.

Klymak, J. M., R. Pinkel, and L. Rainville (2008), Direct breaking of the internal tide near topography: Kaena Ridge, Hawaii, *J. Phys. Oceanogr.*, *38*, 380–399.

Ledwell, J. R., A. J. Watson, and C. S. Law (1993), Evidence for slow mixing across the pycnocline from an open–ocean tracer–release experiment, *Nature*, *364*, 701–703.

Legg, S., and A. Adcroft (2003), Internal wave breaking at concave and convex continental slopes, *J. Phys. Oceanogr.*, *33*, 2224–2246.

Leifer, I., P. B. Luyendyk, J. Boles, and J. F. Clark (2006), Natural marine seepage blowout: Contribution to atmospheric methane, *Global Biogeochem. Cycles*, *20*, GB3008, doi:10.1029/2005GB002668.

Linke, P., S. Sommer, L. Rovelli, and D. F. McGinnis (2010), Physical limitations of dissolved methane fluxes: The role of bottom-boundary layer processes, *Mar. Geol.*, *272*, 209–222.

Lorke, A. (2007), Boundary mixing in the thermocline of a large lake, *J. Geophys. Res.*, *112*, C09019, doi:10.1029/2006JC004008.

McDougall, T. J., R. Feistel, F. J. Millero, D. R. Jackett, D. G. Wright, B. A. King, G. M. Marion, C.-T. A. Chen, and P. Spitzer (2009), Calculation of the thermodynamic properties of seawater, Global ship-based repeat hydrography manual, IOCCP Rep. 14, pp. 131, ICPO Publ. Ser. 134, UNESCO, Paris.

McGinnis, D. F., A. Lorke, A. Wüest, A. Stöckli, and J. C. Little (2004), Interaction between a bubble plume and the near field in a stratified lake, *Water Resour. Res.*, *40*, W10206, doi:10.1029/2004WR003038.

Munk, W. (1966), Abyssal recipes, *Deep Sea Res.*, *13*, 707–730.

Munk, W., and C. Wunsch (1998), Abyssal recipes. II: Energetics of tidal and wind mixing, *Deep Sea Res. Part I*, *45*, 1977–2010.

Naudts, L., J. Greinert, J. Poort, J. Belza, E. Vangampelaere, D. Boone, P. Linke, J. P. Henriet, and M. De Batist (2010), Active venting seep sites on the gas-hydrate-bearing Hikurangi Margin, off New Zealand: Visual observations and measurements, *Mar. Geol.*, *272*, 233–250.

Osborn, T. R. (1980), Estimates of the local rate of vertical diffusion from dissipation measurements, *J. Phys. Oceanogr.*, *10*, 83–89.

Reeburgh, W. S. (2007), Oceanic methane biogeochemistry, *Chem. Rev.*, *107*, 486–513.

Rehder, G., I. Leifer, P. G. Brewer, G. Friederich, and E. T. Peltzer (2009), Controls on methane bubble dissolution inside and outside the hydrate stability field from open ocean field experiments and numerical modeling, *Mar. Chem.*, *114*, 19–30.

Rudnick, D. L., and R. Ferrari (1999), Compensation of horizontal temperature and salinity gradients in the ocean mixed layer, *Science*, *283*, 526–529.

Sauter, E. J., S. I. Muyakshin, J.-L. Charlou, S. Schlüter, A. Boetius, K. Jerosch, E. Damm, J.-P. Foucher, and M. Klages (2006), Methane discharge from a deep-sea submarine mud volcano into the upper water column by gas hydrate-coated methane bubbles, *Earth Planet. Sci. Lett.*, *243*, 354–365.

Schmitt, R. W. (1999), Spice and the demon, *Science*, *283*, 498–499.

Schneider von Deimling, J., J. Greinert, N. R. Chapman, W. Rabbel, and P. Linke (2010), Acoustic imaging of natural gas bubble ebullition in the North Sea: Sensing the temporal, spatial and activity variability, *Limnol. Oceanogr. Methods*, *8*, 155–171.

Schneider von Deimling, J., G. Rehder, J. Greinert, D. F. McGinnnis, A. Boetius, and P. Linke (2011), Quantification of seep-related methane gas emissions at Tommeliten, *North Sea, Cont. Shelf Res.*, *31*, 867–878.

Stommel, H. M. (1993), A conjectural regulating mechanism for determining the thermohaline structure of the oceanic mixed layer, *J. Phys. Oceanogr.*, *23*, 142–148.

TEOS (2010). [Available at http://www.teos-10.org/, accessed 29 May 2013.]

Thorpe, S. A. (1977), Turbulence and mixing in a Scottish loch, *Philos. Trans. R. Soc. London A*, *286*, 125–181.

Thorpe, S. A. (1987a), Transitional phenomena and the development of turbulence in stratified fluids: A review, *J. Geophys. Res.*, *92*, 5231–5248.

Thorpe, S. A. (1987b), Current and temperature variability on the continental slope, *Philos. Trans. R. Soc. London A*, *323*, 471–517.

van Haren, H. (2006), Nonlinear motions at the internal tide source, *Geophys. Res. Lett.*, *33*, L11605, doi:10.1029/2006GL025851.

van Haren, H. (2007), Shear at the critical diurnal latitude, *Geophys. Res. Lett.*, *34*, L06601, doi:10.1029/2006GL028716.

van Haren, H. (2009), Using high-sampling rate ADCP for observing vigorous processes above sloping [deep] ocean bottoms, *J. Mar. Syst.*, *77*, 418–427.

van Haren, H., and C. Millot (2006), Determination of buoyancy frequency in weakly stable waters, *J. Geophys. Res.*, *111*, C03014, doi:10.1029/2005JC003065.

van Haren, H., and C. Millot (2009), Slantwise convection: A candidate for homogenization of deep newly formed dense waters, *Geophys. Res. Lett.*, *36*, L12604, doi:10.1029/2009GL038736.

van Haren, H., and L. Gostiaux (2010), A deep-ocean Kelvin-Helmholtz billow train, *Geophys. Res. Lett.*, *37*, L03605, doi:10.1029/2009GL041890.

van Haren, H., and L. Gostiaux (2012), Detailed internal wave mixing above a deep-ocean slope, *J. Mar. Res.*, *70*, 173–197.

van Haren, H., M. Laan, D.-J. Buijsman, L. Gostiaux, M. G. Smit, and E. Keijzer (2009), NIOZ3: Independent temperature sensors sampling yearlong data at a rate of 1 Hz, *IEEE J. Oceanic Eng.*, *34*, 315–322.

Westbrook, G. K., et al. (2009), Escape of methane gas from the seabed along the West Spitsbergen continental margin, *Geophys. Res. Lett.*, *36*, L15608, doi:10.1029/2009GL039191.